



# Time-dependent, non-monotonic response of warm convective cloud fields to changes in aerosol loading

Guy Dagan, Ilan Koren, Orit Altaratz, and Reuven H. Heiblum

Department of Earth and Planetary Sciences, The Weizmann Institute of Science, Rehovot 76100, Israel

Correspondence to: Ilan Koren (ilan.koren@weizmann.ac.il)

Received: 14 August 2016 – Discussion started: 24 August 2016

Revised: 23 May 2017 – Accepted: 24 May 2017 – Published: 20 June 2017

**Abstract.** Large eddy simulations (LESs) with bin microphysics are used here to study cloud fields' sensitivity to changes in aerosol loading and the time evolution of this response. Similarly to the known response of a single cloud, we show that the mean field properties change in a non-monotonic trend, with an optimum aerosol concentration for which the field reaches its maximal water mass or rain yield. This trend is a result of competition between processes that encourage cloud development versus those that suppress it. However, another layer of complexity is added when considering clouds' impact on the field's thermodynamic properties and how this is dependent on aerosol loading. Under polluted conditions, rain is suppressed and the non-precipitating clouds act to increase atmospheric instability. This results in warming of the lower part of the cloudy layer (in which there is net condensation) and cooling of the upper part (net evaporation). Evaporation at the upper part of the cloudy layer in the polluted simulations raises humidity at these levels and thus amplifies the development of the next generation of clouds (preconditioning effect). On the other hand, under clean conditions, the precipitating clouds drive net warming of the cloudy layer and net cooling of the sub-cloud layer due to rain evaporation. These two effects act to stabilize the atmospheric boundary layer with time (consumption of the instability). The evolution of the field's thermodynamic properties affects the cloud properties in return, as shown by the migration of the optimal aerosol concentration toward higher values.

## 1 Introduction

Despite the extensive research conducted in the last few decades and the fact that clouds have an important role in the Earth's energy balance (Trenberth et al., 2009), clouds are still considered to be one of the largest sources of uncertainty in the study of climate and climate change (Forster et al., 2007; Boucher et al., 2013).

Warm-cloud (containing liquid water only) formation depends on the availability of water vapor and aerosols acting as cloud condensation nuclei (CCN). Changes in aerosol concentration modulate the cloud droplet size distribution and total number. Polluted clouds (forming under high aerosol loading) initially have smaller and more numerous droplets, with a narrower size distribution compared to clean clouds (Squires, 1958; Squires and Twomey, 1960; Warner and Twomey, 1967; Fitzgerald and Spysers-Duran, 1973).

The initial droplet size distribution affects key cloud processes such as condensation–evaporation, collision–coalescence and sedimentation. The condensation–evaporation process is proportional to the total droplet surface area, which increases with the droplet number concentration (for a given total liquid water mass). Under given supersaturation conditions, the condensation in polluted clouds is more efficient (higher condensation rate or shorter consumption time of the supersaturation – Pinsky et al., 2013; Seiki and Nakajima, 2014; Koren et al., 2014; Kogan and Martin, 1994; Dagan et al., 2015a). However, under subsaturation conditions, for the same reason, it implies higher evaporation efficiency. The evaporation induces downdrafts and stronger vorticity and hence can lead to stronger mixing of the cloud with its environment in polluted conditions (Xue and Feingold, 2006; Jiang et al., 2006; Small et al., 2009).

The initiation of collision–coalescence is delayed in polluted clouds (Gunn and Phillips, 1957; Squires, 1958; Albrecht, 1989). This drives a delay in rain formation and can affect the amount of surface rain (Rosenfeld, 1999, 2000; Cheng et al., 2007; Khain, 2009; Levin and Cotton, 2009; Koren et al., 2012; Hazra et al., 2013a, b; Dagan et al., 2015b).

Aerosol effects on single warm convective clouds were shown to have an optimal value with respect to maximal water mass, cloud depth and rain yield (Dagan et al., 2015a, b), which depends on the environmental conditions. For aerosol concentrations lower than the optimum, the positive relationship between aerosol concentration and cloud development is a result of two main processes: (1) a larger latent heat release driven by the increase in the condensation efficiency causing stronger updrafts and (2) a decrease in the effective terminal velocity ( $|\eta|$ , i.e. mass-weighted terminal velocity of the hydrometeors) (Koren et al., 2015) due to initial smaller droplets and the delay in the collision–coalescence process. The smaller droplets have higher mobility (the water mass moves up better with surrounding updraft), reaching higher into the atmosphere and prolonging the cloud growth.

For aerosol concentration values above the optimum, the suppressing aerosol effects take over, namely (1) stronger mixing of the cloud with its environment driven by the increased evaporation efficiency (Small et al., 2009) and (2) an increased water-loading effect due to the rain suppression.

Understanding the overall aerosol effect is even more complex when considering processes on the cloud field scale. Clouds affect the surrounding thermodynamic conditions by changing the humidity and temperature profiles (Lee et al., 2014; Seifert et al., 2015; Stevens and Feingold, 2009; Saleeby et al., 2015). In addition, clouds affect the solar and longwave radiation budgets in the field. Over land the radiation effects change the surface temperature and therefore can significantly affect heat and moisture fluxes and as a result the cloud properties (Koren et al., 2004, 2008a; Feingold et al., 2005).

The invigoration mechanism, which refers to deeper and larger clouds with larger mass that develop under polluted conditions, was studied mainly in deep convective clouds (Andreae et al., 2004; Koren et al., 2005; Rosenfeld et al., 2008; Tao et al., 2012; Fan et al., 2013; Hazra et al., 2013a; Altaratz et al., 2014). Our focus here is on warm-cloud fields for which previous observational studies reported an invigoration effect or a non-monotonic response of the clouds to an increase in aerosol loading. For example, Kaufman et al. (2005) found an increase in cloud fraction (CF) of warm-cloud fields with increasing aerosol loading over the tropical Atlantic Ocean. Yuan et al. (2011) reported that an increase in volcanic aerosols near Hawaii led to increased trade cumulus CF and cloud top height. Dey et al. (2011) have shown that an increase in aerosol optical depth (AOD) from clean to slightly polluted resulted in an increase in CF in warm clouds over the Indian Ocean. An additional increase in the AOD

resulted in a decrease in CF, explained by the semi-direct effect of absorbing aerosols. Costantino and Bréon (2013) reported higher CF over the southeastern Atlantic under high aerosol loading conditions. From convective stability considerations, deeper clouds tend to have a larger area (larger CF). It was shown that warm convective cloud area correlates positively with cloud depth (Benner and Curry, 1998; Koren et al., 2008b).

Koren et al. (2014) have shown that warm convective clouds over the southern oceans can be considered as aerosol limited up to moderate aerosol loading conditions. As the AOD increases, the clouds were shown to be deeper and larger and to produce stronger rain rates. A reversal in the trend of the liquid water path (LWP) as a function of increasing AOD was reported using observations of warm convective clouds under a large range of meteorological conditions (Savane et al., 2015). Li et al. (2011) studied warm clouds over the southern great plains of the United States and reported no aerosol effect on cloud top height.

On the other hand, numerical studies of the aerosol effect on warm cumulus cloud fields show either no effect or cloud suppression (meaning shallower and smaller clouds under higher aerosol loading conditions). Jiang and Feingold (2006) found that the LWP, CF and cloud depth of warm shallow convective clouds are insensitive to an increase in aerosol loading. However, they demonstrated rain suppression by aerosols. Xue et al. (2008) showed smaller clouds and suppression of precipitation in an increased aerosol loading environment. Jiang et al. (2010) found a non-monotonic change in the derivative of the surface rain rate with aerosol loading (susceptibility) for higher maximal LWP clouds but a monotonic decrease in the total precipitation with aerosol loading. Seigel (2014) showed that cloud size decreases with aerosol loading due to enhanced entrainment at the cloud margins.

Some previous studies have demonstrated clouds' alteration of their environment (Zhao and Austin, 2005; Heus and Jonker, 2008; Malkus, 1954; Lee et al., 2014; Zuidema et al., 2012; Roesner et al., 1990). One example of such an effect is the “preconditioning” or “cloud-deepening” effect (Nitta and Esbensen, 1974; Roesner et al., 1990; Stevens, 2007; Stevens and Seifert, 2008), where clouds cool and moisten the upper cloudy and inversion layers and in this way encourage the development of the next generation of clouds that encounter improved environmental conditions. This effect is influenced by the clouds' microphysical properties (Stevens and Feingold, 2009; Saleeby et al., 2015). The role of warm convective clouds in moistening the free troposphere was studied intensively using both observations and cloud field numerical models (Brown and Zhang, 1997; Johnson et al., 1999; Takemi et al., 2004; Kuang and Bretherton, 2006; Holloway and Neelin, 2009; Waite and Khouider, 2010).

Albrecht (1993) used a theoretical single-column model to study the effect of precipitation on the thermodynamic structure of the trade wind boundary layer and found that

even low rain rates can dramatically affect the profiles. Under precipitating conditions, the cloudy layer is warmer, drier and more stable than under non-precipitation conditions. Albrecht (1993) also showed that under non-precipitating conditions the inversion height is greater than under precipitating conditions, due to the larger amount of liquid water evaporating at those elevations.

Another way clouds affect their environment is by the evaporation of rain below the cloud base, which induces cooling of the sub-cloud layer (Zuidema et al., 2012; Heiblum et al., 2016a). Lee et al. (2014) demonstrated the aerosol effects on the field's CAPE (convective available potential energy) (as distributed above cloud base or below it). The organization of the field is influenced by cloud processes as well. Enhanced evaporative cooling in the sub-cloud layer, for example, can produce cold pools which enhance the generation of clouds only at their boundaries and hence change the organization of the field (Seigel, 2014; Seifert and Heus, 2013; Heiblum et al., 2016a).

A recent paper (Dagan et al., 2016) showed that polluted clouds act to increase the thermodynamic instability with time, while clean clouds consume the atmospheric instability. The trend of the pollution-driven increase in the instability is halted once the clouds are thick enough to develop significant precipitation. Indeed, studies of long simulation times (> 30 h) showed that the initial differences between clean and polluted cases are reduced by negative feedbacks of the clouds on the thermodynamic conditions (Lee et al., 2012; Seifert et al., 2015).

In this work we explore the coupled microphysical-dynamic system of warm marine cloud fields using a bin-microphysics scheme under a large range of aerosol concentrations. We study the aerosol–cloud–environmental thermodynamic system by examining how changes in aerosol concentrations affect clouds properties and the related modifications of the thermodynamic conditions over time, which also drive feedbacks on the evolution of cloud properties.

## 2 Methodology

The SAM (System for Atmospheric Modeling), non-hydrostatic, anelastic large eddy simulation (LES) model version 6.10.3 (Khairoutdinov and Randall, 2003) was used to simulate the well-studied trade cumulus case of the Barbados Oceanographic and Meteorological Experiment (BOMEX; Holland and Rasmusson, 1973; Siebesma et al., 2003). The BOMEX case is an idealized trade cumulus cloud field that is based on observations made near Barbados during June 1969. This case was initialized using the setup specified in Siebesma et al. (2003). The setup includes surface fluxes and large-scale forcing (see details in Heiblum et al., 2016b). The horizontal resolution was set to 100 m, while the vertical resolution was set to 40 m. The domain size was  $12.8 \times 12.8 \times 4.0 \text{ km}^3$  and the time step was 1 s. Due to com-

putational limitations, we had to restrict the domain size to a scale that has a limited capability for capturing large-scale organization (Seifert and Heus, 2013). The model ran for 16 h and the statistical analysis included all but the first 2 h (total of 14 h). After 2 h of simulations the initial increase in the total liquid water mass in the domain stopped and the differences between the simulations (difference in relation to the aerosol loading) became significant. Therefore, 2 h is determined as spin-up time (similar to the spin-up time in Xue and Feingold, 2006).

A bin microphysical scheme (Khain and Pokrovsky, 2004) was used. The scheme solves warm microphysical processes, including droplet nucleation, diffusional growth, collision coalescence, sedimentation and breakup.

In order to focus on the aerosol effect on the thermodynamic properties of the field, the radiative effects (as included in the large-scale forcing – see details in Dagan et al., 2016) were prescribed in all simulations. The aerosol distribution adopts a marine size distribution (see details in Jaenicke, 1988, and Altaratz et al., 2008). Eight different simulations were conducted simulating a wide range of aerosol loading conditions from extremely pristine to polluted (total concentration of 5, 25, 50, 100, 250, 500, 2000 and  $5000 \text{ cm}^{-3}$  near ground level; Dagan et al., 2015a). To reduce the results' sensitivity to the shape of the aerosol size distribution and to focus on the aerosol number concentration effect, the different aerosol concentrations are calculated by the multiplication of all bins by a constant factor and maintaining a constant shape of the size distribution. The aerosol is assumed to be composed of ammonium sulfate and initialized with a constant mixing ratio with height. A prognostic equation is solved for the aerosol mass, including regeneration upon evaporation and removal by surface rain. Regeneration upon evaporation of cloud drops was shown to be a very important source of aerosols, especially in polluted conditions (Yin et al., 2005). The aerosol serves as potential cloud condensation nuclei (CCN), and it is activated based on the Köhler theory (the scheme is described in Khain et al., 2000). The aerosol (water drop) size distribution is calculated between 5 nm and  $2 \mu\text{m}$  ( $2 \mu\text{m}$ – $3.2 \text{ mm}$ ). For both aerosol and drops, successive bins represent doubling of the mass.

The effects of changes in aerosol concentration on the drop concentration and its mean size for the different simulations can be found in Fig. S1 in the Supplement.

## 3 Results and discussion

### 3.1 Mean cloud field properties under different aerosol loading conditions

The aerosol effects on the mean field properties during the entire run are examined first, followed by a more detailed examination of the time evolution in the next section. Figure 1 presents mean values of key properties of cloud fields as a

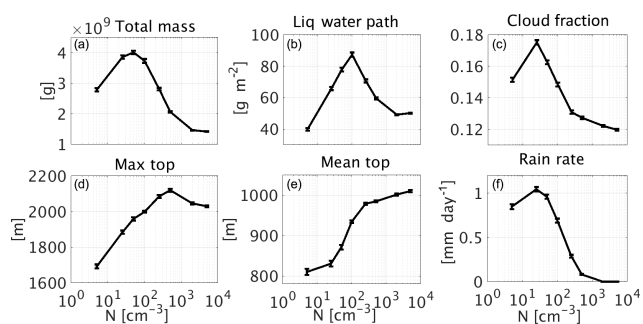


**Figure 1.** Mean properties (over domain and time) of the simulated cloud fields as a function of the aerosol concentration used in the simulation: (a) total liquid water mass in the domain, (b) cloudy LWP, (c) CF for columns with  $\tau > 0.3$ , (d) maximum cloud top, (e) mean cloud top and (f) surface rain rate. Each of these mean properties are calculated for the last 14 h of the 16 h of simulation. The error bars present the standard errors. For details about the different properties see the text.

function of the aerosol loading for the entire (14 h) simulation time.

The total water mass (calculated as mean over time in each domain) as a function of aerosol concentration shows a clear reversal in the trend (Fig. 1a). For the given environmental conditions simulated here, it increases when aerosol loading is increased from 5 to  $50 \text{ cm}^{-3}$ . An additional increase in the aerosol loading results in a decrease in the total water mass in the domain.

The LWP (Fig. 1b) calculated as a mean over time over all cloudy columns in each domain, which is strongly correlated with the total water mass, also shows the same non-monotonic general trend. The maximum in the curve of the cloudy LWP is at a slightly higher aerosol concentration compared to the total mass ( $100 \text{ cm}^{-3}$ ). This difference can be explained by the link to the CF (calculated as the area covered by clouds with optical path  $\tau > 0.3$ ; Fig. 1c) that decreases above an aerosol loading of  $25 \text{ cm}^{-3}$ . Thus, for the more polluted simulations, the mass is distributed on smaller horizontal cloud areas, as shown in previous studies (Seigel, 2014).

There is also a significant difference in the way the water mass is distributed along the atmospheric column in the different simulations. The maximum cloud top height (Fig. 1d), calculated as a mean over time of the altitude of the highest grid box in the domain that contains liquid water content ( $\text{LWC} > 0.01 \text{ g kg}^{-1}$ ), increases significantly when aerosol loading increases up to  $500 \text{ cm}^{-3}$  (an increase from 1692 to 2120 m when aerosol loading increases from 5 to  $500 \text{ cm}^{-3}$ ). An additional increase in the aerosol loading results in a minor decrease in the maximum cloud top height (down to 2030 m for an aerosol loading of  $5000 \text{ cm}^{-3}$ ). The minor decrease seen for this range of aerosol concentration (compared with the larger decrease in the mean LWP for example) can be explained by the location of the maximal cloud top height

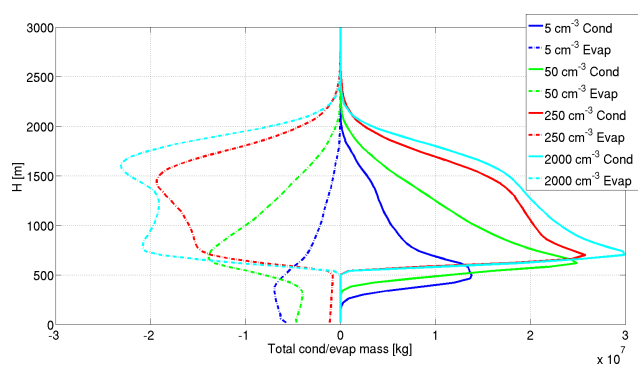


**Figure 2.** Domain's total condensed (solid lines) and evaporated mass (dashed lines) for 14 h of simulation along four different simulations conducted with different aerosol concentration levels ( $5 \text{ cm}^{-3}$  – blue;  $50 \text{ cm}^{-3}$  – green;  $250 \text{ cm}^{-3}$  – red; and  $2000 \text{ cm}^{-3}$  – cyan).

above the cloud core, which is affected mainly by the invigoration processes (enhanced condensation and latent heat release) and less by margin-oriented processes (enhanced entrainment and evaporation) that significantly impact the total cloud mass (Dagan et al., 2015a). Another reason is the cloud-deepening effect under polluted conditions (Stevens, 2007; Seifert et al., 2015) that will be described later. As for the mean cloud top height calculated as a mean of all cloudy columns along the whole run (Fig. 1e), the trend shows a monotonic increase with aerosol loading. The trend is approaching a saturation level for high aerosol concentration values. The mean cloud top value over the simulation is 810 and 1010 m for the simulations with aerosol loading of 5 to  $5000 \text{ cm}^{-3}$ , respectively.

Presenting together the mean over time of the maximum and the mean cloud top height captures, in a compact yet informative, way the response of the cloud top height distribution to changes in aerosol loading and reduces the sensitivity to outliers. Moreover, by averaging over time, the significance of the outliers is decreased as well.

The trend in the domain's average rain rate, as a function of the aerosol loading (Fig. 1f), shows a peak at a relatively low aerosol loading (similar to the optimal value of the CF) of  $25 \text{ cm}^{-3}$ .

Figure 2 presents the vertical profiles of the total condensed and evaporated mass during the simulations for four different simulations. We note that as the aerosol loading increases, both the condensed and evaporated mass increased (this is due to the increase in the diffusion rates – see Fig. S2 – and despite the decrease in cloud fraction – see Fig. 1c; Dagan et al., 2015a; Koren et al., 2014; Pinsky et al., 2013; Seiki and Nakajima, 2014). Below the cloud base (located around 550 m), the clean simulations have small rain evaporation values which are absent in the polluted simulations.

Effective terminal velocity ( $\eta$ ) is defined as the mass-weighted average terminal velocity of all the hydrometeors

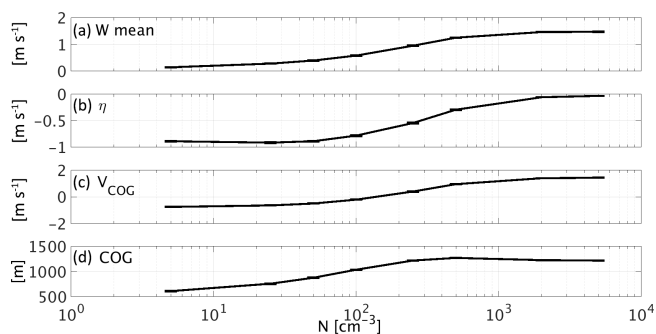


**Figure 3.** Mean (over time and space) of (a) updraft ( $W$ ), (b) effective terminal velocity ( $\eta$ ), (c) the center of gravity velocity  $V_{\text{COG}}$  and (d) COG (center of gravity) height as a function of the aerosol concentration. All calculated for the last 14 h of the 16 h of simulation.

within a given volume of air (Koren et al., 2015). By definition,  $\eta$  measures the terminal velocity of the water mass's center of gravity (COG), i.e. the COG's movement with respect to the surrounding air's vertical velocity ( $W$ ). Small absolute values  $|\eta|$  imply that the droplets' COG will move better with the surrounding air; i.e. the droplets will have better mobility (Koren et al., 2015). The sum  $V_{\text{COG}} = W + \eta$  ( $\eta$  always negative) reflects the water mass COG vertical velocity relative to the surface. Positive  $V_{\text{COG}}$  implies a rise in the COG, and a negative value means a fall.

The mean updraft (in both space and time, weighted by the liquid water mass in each grid box to be consistent with the COG point of view – Fig. 3a) increases with the increase in aerosol loading, in agreement with previous studies (Saleeby et al., 2015; Seigel, 2014). This indicates an increase in the latent heat contribution to the cloud buoyancy, driven by an increase in the condensation efficiency (Dagan et al., 2015a, b; Koren et al., 2014; Pinsky et al., 2013; Seiki and Nakajima, 2014) (Figs. 2 and S2). At the same time,  $|\eta|$  decreases as the aerosol concentration increases (Fig. 3b) indicating better mobility of the smaller droplets, allowing them to move more easily with the air's updraft. The outcome of these two effects is an increased  $V_{\text{COG}}$  for a higher aerosol concentration (Fig. 3c), indicating that the polluted clouds' liquid water is pushed higher within the atmosphere (Koren et al., 2015) as shown by higher COG (Fig. 3d).

The mean COG height of the water mass (Grabowski et al., 2006; Koren et al., 2009) (Fig. 3d), increases with the aerosol loading up to a relatively high concentration ( $500 \text{ cm}^{-3}$ ). Note that while the trend in the system's characteristic velocities ( $\eta$  and  $W$ ) is a monotonic increase, the COG has an optimal aerosol concentration for which it reaches its maximum height ( $500 \text{ cm}^{-3}$ ). For aerosol concentrations above  $500 \text{ cm}^{-3}$ , a minor decrease is shown. As described above, the COG height increase with aerosol loading, between extremely clean and polluted conditions, can be explained by increased  $V_{\text{COG}}$ , which is a product of both lower  $|\eta|$  and

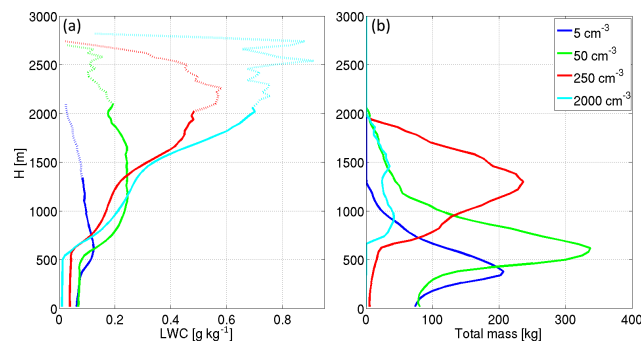


**Figure 4.** (a) Mean LWC vertical profiles. (b) Vertical profiles of the mean (over time) total liquid water mass per height for four different simulations ( $5 \text{ cm}^{-3}$  – blue;  $50 \text{ cm}^{-3}$  – green;  $250 \text{ cm}^{-3}$  – red; and  $2000 \text{ cm}^{-3}$  – cyan). The mean profiles are calculated for the last 14 h of the 16 h of simulation. Note that dotted parts of the curves in (a) represents heights at which the total liquid water mass was less than 1 % of the maximum total mass (Fig. 4b).

increased updraft on the cloud scale and larger thermodynamic instability induced by the polluted clouds on the field scale as will be shown in the next section (Dagan et al., 2016; Heiblum et al., 2016a). The reduction in the mean COG height in the most polluted simulations is caused by cloud-suppressing processes, including an enhanced entrainment (see the enhanced evaporation efficiency with aerosol loading – Figs. 2, S2) and larger water loading (Dagan et al., 2015a – shown also in Fig. 4a below).

The trend in COG height can be also viewed (in more detail) in Fig. 4a, which presents profiles of mean LWC for cloudy voxels only.

We show that both the height and the magnitude of the maximum LWC increase with the aerosol loading. This is due to both rain suppression (Fig. 1f) and an increased  $V_{\text{COG}}$  (Fig. 3c) with aerosol loading. There is a reduction in the mean LWP (for  $> 100 \text{ cm}^{-3}$  – Fig. 1b) although there is an increase in the LWC with aerosol loading due to the differences in cloud fraction (Fig. 1c) and in the vertical distribution of the liquid water (Fig. 4b). At the upper part of the clouds ( $H > 2000 \text{ m}$ ), in the polluted case, a small amount of cloudy pixels have a large mean LWC (and hence a large water-loading effect), but the total amount of liquid water is small (Fig. 4b). Below the cloud base ( $H < \sim 550 \text{ m}$ ) the LWC trend is reversed due to the enhancement of rain in the clean runs (Fig. 1f). The increase in LWC with aerosol loading implies a larger water-loading negative component in the clouds' buoyancy.

All the evidence presented in Figs. 2–4 explains the non-monotonic trends in the cloud properties' response to changes in aerosol loading (Fig. 1). For clean conditions (below the optimal aerosol concentration value), an increase in aerosol loading would enhance the cloud development (larger mass, LWP, cloud top, CF, rain rate) because of two main factors: (1) an increase in the condensation efficiency

(due to the larger total droplet surface area for condensation and longer time – Figs. 2, S2) and (2) smaller effective terminal velocity ( $|\eta|$ ) values, which, per given updraft, allow a cloud's hydrometeors to be pushed higher within the atmosphere (Koren et al., 2015) (Fig. 3b).

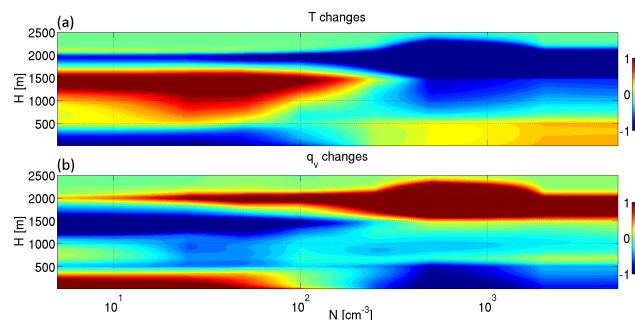
The higher condensation efficiency in polluted clouds (Fig. 2) results in a larger latent heat release that enhances the updraft (Fig. 3a) and cloud development. The increased  $V_{\text{COG}}$  reflects the two cloud-enhancing processes (decrease in  $|\eta|$  and larger mean updraft). We note that the increase in the mean updraft values with aerosol loading is seen despite the negative effect of water loading (see Fig. 4a). For aerosol concentrations above the optimum, cloud development is suppressed by the increase in evaporation efficiency (Fig. 2) and hence stronger mixing of the cloud with its environment (i.e. Small et al., 2009) and larger water loading due to rain suppression (Dagan et al., 2015a, Fig. 4a).

### 3.2 The time evolution of the mean cloud field properties under different aerosol loading conditions

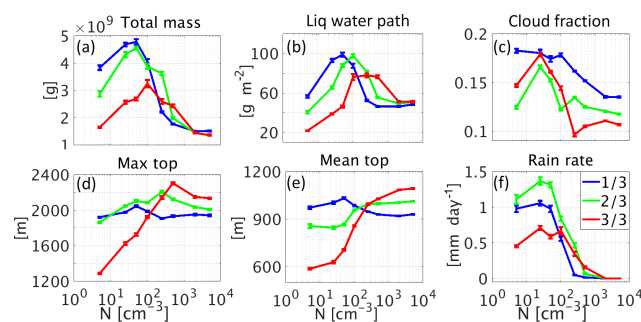
All the aerosol effects that were discussed up to this point (condensation–evaporation efficiencies,  $\eta$  and water loading) are applicable both on the single-cloud scale as well as on the cloud field scale. However, on the cloud field scale, another aspect needs to be considered, namely the time evolution of the effect of clouds on the field's thermodynamic conditions (which was the focus of a recent study by Dagan et al., 2016).

Figure 5 presents the changes (final value minus initial one) in the temperature ( $T$ ) and water vapor content ( $q_v$ ) vertical profiles as a function of aerosol concentration used in the simulation. The initial profiles were identical in all simulations. Figure S3 presents the full temporal evolution of those parameters. In low aerosol concentration runs ( $100 \text{ cm}^{-3}$  and below), the sub-cloud layer becomes cooler and wetter with time and the cloudy layer warmer and drier. Meanwhile, under higher aerosol concentrations conditions ( $250 \text{ cm}^{-3}$  and above), the sub-cloud layer becomes warmer and drier while the cloudy and inversion layers become colder and wetter. This trend is driven by the condensation–evaporation tendencies along the vertical profile (see Fig. 2; Dagan et al., 2016). Under low aerosol concentration conditions, water condenses at the cloudy layer and is advected downward to the sub-cloud layer where it partially evaporates. Under polluted conditions, on the other hand, the condensed water from the lower part of the cloudy layer is advected up to the upper cloudy and inversion layers (driven by larger  $V_{\text{COG}}$  – Fig. 3) and evaporates there (Dagan et al., 2016).

Such trends in the environmental thermodynamic conditions are likely to affect the formation of clouds. In Fig. 6 the time evolution of some of the key cloud field properties is considered (the same properties that were shown in Fig. 1). The blue, green and red curves represent the mean values



**Figure 5.** Total change, during 16 h of simulation in the temperature (K; **a**) and water vapor content ( $\text{g kg}^{-1}$ ; **b**) domain mean vertical profiles as a function of the aerosol concentration used in the simulation.



**Figure 6.** Mean properties (over time and domain) of the simulated cloud fields as a function of the aerosol concentration used in the simulation: **(a)** total liquid water mass in the domain, **(b)** cloudy LWP, **(c)** CF for columns with  $\tau > 0.3$ , **(d)** maximum cloud top, **(e)** mean cloud top and **(f)** surface rain rate. Each property is calculated separately for each period of one-third of the simulations (blue, green and red for the first, second and third periods, respectively). The error bars present the standard error. For details about the different properties, see the text.

over the first, second and third periods of the simulations, respectively (each one covers 4 h and 40 min). Table 1 presents change (in percentage) in the mean values of key variables between the third period of the eight simulations (11 h 20 min to 16 h into the simulation; red curves in Fig. 6) and the first period (2 h to 6 h 40 min into the simulation; blue curves in Fig. 6).

The examination of the evolution of the mean total water mass along the simulations (Fig. 6a; blue, green and red curves) presents a different trend between the clean and the polluted simulations. In the clean simulations ( $5\text{--}100 \text{ cm}^{-3}$ ) the total water mass decreases significantly with time (a decrease of 57, 45, 44 and 20 % in total mass for the cases of 5, 25, 50 and  $100 \text{ cm}^{-3}$ , respectively – see Table 1). On the other hand, in the more polluted simulations, (with an aerosol loading of 250 and  $500 \text{ cm}^{-3}$ ), there is an increase in the total water mass with time (of 17 and 37 % between the first and the last periods of the simulations, respectively). Under

**Table 1.** Change (in %) in key variables between the mean values in the last period of the simulations and the first period. Negative values are presented in bold.

|                       | Total mass (%) | LWP (%)      | COG (%)      | Max top (%)  | Mean top (%) | W max (%)    | CF (%)       | Rain rate (%) |
|-----------------------|----------------|--------------|--------------|--------------|--------------|--------------|--------------|---------------|
| 5 cm <sup>-3</sup>    | <b>-57.0</b>   | <b>-61.4</b> | <b>-43.1</b> | <b>-32.9</b> | <b>-39.7</b> | <b>-28.2</b> | <b>-19.7</b> | <b>-53.5</b>  |
| 25 cm <sup>-3</sup>   | <b>-45.2</b>   | <b>-58.3</b> | <b>-39.6</b> | <b>-17.8</b> | <b>-37.4</b> | <b>-38.8</b> | <b>-0.6</b>  | <b>-32.9</b>  |
| 50 cm <sup>-3</sup>   | <b>-43.8</b>   | <b>-53.1</b> | <b>-33.7</b> | <b>-15.6</b> | <b>-31.6</b> | <b>-47.9</b> | <b>-7.5</b>  | <b>-40.1</b>  |
| 100 cm <sup>-3</sup>  | <b>-20.1</b>   | <b>-13.0</b> | <b>-16.1</b> | <b>-3.2</b>  | <b>-13.0</b> | <b>-32.8</b> | <b>-19.0</b> | 19.6          |
| 250 cm <sup>-3</sup>  | 17.5           | 48.6         | 5.0          | 12.4         | 5.0          | <b>-4.3</b>  | <b>-40.7</b> | 598.1         |
| 500 cm <sup>-3</sup>  | 37.4           | 64.2         | 19.9         | 19.2         | 10.7         | 9.4          | <b>-30.9</b> | 841.5         |
| 2000 cm <sup>-3</sup> | <b>-3.7</b>    | 10.6         | 14.8         | 10.1         | 17.9         | 6.0          | <b>-17.8</b> | –             |
| 5000 cm <sup>-3</sup> | <b>-10.1</b>   | 5.7          | 13.7         | 9.9          | 17.5         | 2.9          | <b>-20.7</b> | –             |

extremely polluted conditions of 2000 and 5000 cm<sup>-3</sup>, the total water mass in the domain is small and there is little change with time. These changes in time push the optimum aerosol concentration to higher values along the simulation time. This trend is also shown for the optimum aerosol concentration with regard to the mean cloudy LWP (Fig. 6b), maximum top (Fig. 6d) and mean top (Fig. 6e).

Trends in the mean rain rate show that in the cleanest simulations (5, 25 and 50 cm<sup>-3</sup>), the rate decreases with time (Fig. 6f; 53.3, 32.9 and 40.1 %, respectively). In the regime of medium to fairly high aerosol loading (100, 250 and 500 cm<sup>-3</sup>), the rain rate increases (19.6, 598.1 and 841.5 %, respectively). And in the most polluted simulations (2000 and 5000 cm<sup>-3</sup>), the surface rain is negligible throughout the simulation time. These trends are explained below.

The time evolution of the thermodynamic conditions (Fig. 5) shows a reduction (enhancement) in the thermodynamic instability with time in the clean (polluted) simulations. Figure 6 and Table 1 indicate that under clean conditions the decrease in the thermodynamic instability with time leads to a decrease in the mean cloud field properties such as total mass, cloud top height and rain rate. Under polluted conditions the trends are opposite and the mean cloud field properties increase with time due to the increase in thermodynamic instability (Dagan et al., 2016) and due to the cloud deepening (Stevens and Seifert, 2008; Stevens, 2007; Seifert et al., 2015). These differences between the clean and polluted simulations drive changes in the optimum aerosol concentration with time. For example, for the LWP (Fig. 1b) the optimum aerosol concentration is 50, 100 and 250 cm<sup>-3</sup> for the first, second and third parts of the simulation, respectively.

#### 4 Summary

Cloud processes can be divided in a simplistic manner into two characteristic scales – the cloud scale and the field scale. Here, using LES model with a bin microphysical scheme we studied the outcome of the processes of the two scales acting

together. We first presented domain-averaged properties over the whole simulation time (Sect. 3.1) to indicate the general aerosol effects in a first-order manner, and then we followed the time evolution of the effects (Sect. 3.2).

A non-monotonic aerosol effect was reported recently for a single-cloud scale (Dagan et al., 2015a, b). Here we show that these trends “survived” the domain and time averaging. We argue that the trend of an enhanced development is driven by two main processes of enhanced condensation and reduced effective terminal velocity (which improves the droplets’ mobility). These processes are mainly related to the core of the clouds and to the early stages of cloud development. We show that the cloud systems characteristic velocities can capture these effects. The effective terminal velocity ( $\eta$ ) inversely measures the mobility. Smaller droplets with smaller variance will have smaller  $|\eta|$  and therefore will be pushed higher in a given updraft, whereas larger droplets with larger  $|\eta|$  will move downward with respect to the surrounding air. An increase in condensation efficiency drives more latent heat release, which enhances the cloud updraft. We showed that  $V_{\text{COG}}$  is a product of the two velocities.

The descending branch in which an increase in aerosol loading suppresses cloud development is governed by an increase in the evaporation efficiency of the subsaturated parts of the clouds and by an increase in water loading.

Since clouds change the atmospheric thermodynamic conditions in which they form, different initial clouds would cause a different impact on the environment. Therefore, the cloud field is a continuously evolving system for which aerosol properties determine an important part of the temporal trends. Figure 5 shows striking differences between the evolution of the thermodynamic profiles in clean and polluted cases. For the polluted clouds (mostly non-precipitating), the upper cloudy layer turns wetter and cooler due to enhanced evaporation and the sub-cloud layer becomes warmer and drier; together, these developments act to increase the instability. On the other hand, clean precipitating clouds consume the initial instability with time by warming

the cloudy layer (due to latent heat release) and cooling the sub-cloud layer by the evaporation of rain.

The polluted cloud feedbacks on the thermodynamic conditions act to deepen the clouds. Since clouds that form in a more unstable environment are expected to be aerosol limited up to higher aerosol concentrations (Koren et al., 2014; Dagan et al., 2015a), an increase in the domain's instability for the polluted cases drives an increase in the optimal aerosol concentration with time.

We note that such an increase in the instability cannot last forever. A deepened cloud will eventually produce larger precipitation rates that may weaken the overall effect on the field (Stevens and Feingold, 2009; Seifert et al., 2015). These results pose an interesting question on the dynamical state of cloud fields in nature. Do the cloud fields “manage” to reach a “near-equilibrium” state (Seifert et al., 2015), for which the deepening effect balances the aerosol effect fast enough that the effects are buffered most of the time (Stevens and Feingold, 2009). Or maybe, the characteristic lifetime of a trade cumulus cloud field is shorter than the time it takes to significantly balance the aerosol effects. In this case the cloud fields could be regarded as “transient”, and therefore, as shown here, aerosol might have a strong effect on the clouds, both through affecting the microphysics, initiating many feedbacks on the cloud scale, and by affecting the field thermodynamic evolution over time.

*Data availability.* Information about the model and initialization files are available upon request to the contact author.

**The Supplement related to this article is available online at <https://doi.org/10.5194/acp-17-7435-2017-supplement>.**

*Competing interests.* The authors declare that they have no conflict of interest.

*Acknowledgements.* This research has been supported by the Minerva foundation with funding from the Federal German Ministry of Education and Research.

Edited by: Barbara Ervens

Reviewed by: two anonymous referees

## References

- Albrecht, B. A.: Aerosols, cloud microphysics, and fractional cloudiness, *Science*, 245, 1227–1230, 1989.
- Albrecht, B. A.: Effects of precipitation on the thermodynamic structure of the trade wind boundary layer, *J. Geophys. Res.-Atmos.*, 98, 7327–7337, 1993.

- Altaratz, O., Koren, I., Reisin, T., Kostinski, A., Feingold, G., Levin, Z., and Yin, Y.: Aerosols' influence on the interplay between condensation, evaporation and rain in warm cumulus cloud, *Atmos. Chem. Phys.*, 8, 15–24, <https://doi.org/10.5194/acp-8-15-2008>, 2008.
- Altaratz, O., Koren, I., Remer, L., and Hirsch, E.: Review: Cloud invigoration by aerosols – Coupling between microphysics and dynamics, *Atmos. Res.*, 140, 38–60, 2014.
- Andreae, M. O., Rosenfeld, D., Artaxo, P., Costa, A. A., Frank, G. P., Longo, K. M., and Silva-Dias, M. A. F.: Smoking rain clouds over the Amazon, *Science*, 303, 1337–1342, <https://doi.org/10.1126/science.1092779>, 2004.
- Benner, T. C. and Curry, J. A.: Characteristics of small tropical cumulus clouds and their impact on the environment, *J. Geophys. Res.*, 103, 28753–28767, <https://doi.org/10.1029/98JD02579>, 1998.
- Boucher, O., Randall, D., Artaxo, P., Bretherton, C., Feingold, G., Forster, P., Kerminen, V., Kondo, Y., Liao, H., Lohmann, U., Rasch, P., Satheesh, S. K., Sherwood, S., Stevens, B., and Zhang, X. Y.: 2013: Clouds and Aerosols. In: *Climate Change 2013: The Physical Science Basis. Contribution of Working Group I to the Fifth Assessment Report of the Intergovernmental Panel on Climate Change*, edited by: Stocker, T. F., Qin, D., Plattner, G.-K., Tignor, M., Allen, S. K., Boschung, J., Nauels, A., Xia, Y., Bex, V., and Midgley, P. M., Cambridge University Press, Cambridge, United Kingdom and New York, NY, USA, 571–657, 2013.
- Brown, R. G. and Zhang, C.: Variability of midtropospheric moisture and its effect on cloud-top height distribution during TOGA COARE, *J. Atmos. Sci.*, 54, 2760–2774, 1997.
- Cheng, C.-T., Wang, W.-C., and Chen, J.-P.: A modelling study of aerosol impacts on cloud microphysics and radiative properties, *Q. J. Roy. Meteor. Soc.*, 133, 283–297, 2007.
- Costantino, L. and Bréon, F.-M.: Aerosol indirect effect on warm clouds over South-East Atlantic, from co-located MODIS and CALIPSO observations, *Atmos. Chem. Phys.*, 13, 69–88, <https://doi.org/10.5194/acp-13-69-2013>, 2013.
- Dagan, G., Koren, I., and Altaratz, O.: Competition between core and periphery-based processes in warm convective clouds – from invigoration to suppression, *Atmos. Chem. Phys.*, 15, 2749–2760, <https://doi.org/10.5194/acp-15-2749-2015>, 2015a.
- Dagan, G., Koren, I., and Altaratz, O.: Aerosol effects on the timing of warm rain processes, *Geophys. Res. Lett.*, 42, 4590–4598, <https://doi.org/10.1002/2015GL063839>, 2015b.
- Dagan, G., Koren, I., Altaratz, O., and Heiblum, R. H.: Aerosol effect on the evolution of the thermodynamic properties of warm convective cloud fields, *Scientific Reports*, 38769, <https://doi.org/10.1038/srep38769>, 2016.
- Dey, S., Di Girolamo, L., Zhao, G., Jones, A. L., and McFarquhar, G. M.: Satellite-observed relationships between aerosol and trade-wind cumulus cloud properties over the Indian Ocean, *Geophys. Res. Lett.*, 38, L01804, <https://doi.org/10.1029/2010GL045588>, 2011.
- Fan, J., Leung, L. R., Rosenfeld, D., Chen, Q., Li, Z., Zhang, J., and Yan, H.: Microphysical effects determine macrophysical response for aerosol impacts on deep convective clouds, *P. Natl. Acad. Sci. USA*, 110, E4581–E4590, 2013.
- Feingold, G., Jiang, H. L., and Harrington, J. Y.: On smoke suppression of clouds in Amazonia, *Geophys. Res. Lett.*, 32, L02804, <https://doi.org/10.1029/2004gl021369>, 2005.



- Fitzgerald, J. and Spyers-Duran, P.: Changes in cloud nucleus concentration and cloud droplet size distribution associated with pollution from St. Louis, *J. Appl. Meteorol.*, 12, 511–516, 1973.
- Forster, P., Ramaswamy, V., Artaxo, P., Bernsten, T., Betts, R., Fahey, D. W., Haywood, J., Lean, J., Lowe, D. C., Myhre, G., Nganga, J., Prinn, R., Raga, G., Schulz, M., and Dorland, R. V.: Changes in Atmospheric Constituents and in Radiative Forcing, in: *Climate Change 2007: The Physical Science Basis. Contribution of Working Group I to the Fourth Assessment Report of the Intergovernmental Panel on Climate Change*, edited by: Solomon, S., Qin, D., Manning, M., Chen, Z., Marquis, M., Averyt, K. B., Tignor, M., and Miller, H. L., Cambridge University Press, Cambridge, United Kingdom and New York, NY, USA, 2007.
- Grabowski, W., Bechtold, P., Cheng, A., Forbes, R., Halliwell, C., Khairoutdinov, M., Lang, S., Nasuno, T., Petch, J., and Tao, W. K.: Daytime convective development over land: A model inter-comparison based on LBA observations, *Q. J. Roy. Meteor. Soc.*, 132, 317–344, 2006.
- Gunn, R. and Phillips, B.: An experimental investigation of the effect of air pollution on the initiation of rain, *J. Meteorol.*, 14, 272–280, 1957.
- Hazra, A., Goswami, B., and Chen, J.-P.: Role of interactions between aerosol radiative effect, dynamics, and cloud microphysics on transitions of monsoon intraseasonal oscillations, *J. Atmos. Sci.*, 70, 2073–2087, 2013a.
- Hazra, A., Mukhopadhyay, P., Taraphdar, S., Chen, J. P., and Cotton, W. R.: Impact of aerosols on tropical cyclones: An investigation using convection-permitting model simulation, *J. Geophys. Res.-Atmos.*, 118, 7157–7168, 2013b.
- Heiblum, R. H., Altaratz, O., Koren, I., Feingold, G., Kostinski, A. B., Khain, A. P., Ovchinnikov, M., Fredj, E., Dagan, G., and Pinto, L.: Characterization of cumulus cloud fields using trajectories in the center-of-gravity vs. water mass phase space. Part II: Aerosol effects on warm convective clouds, *J. Geophys. Res.-Atmos.*, 121, 6356–6373, 2016a.
- Heiblum, R. H., Altaratz, O., Koren, I., Feingold, G., Kostinski, A. B., Khain, A. P., Ovchinnikov, M., Fredj, E., Dagan, G., and Pinto, L.: Characterization of cumulus cloud fields using trajectories in the center of gravity versus water mass phase space: 1. Cloud tracking and phase space description, *J. Geophys. Res.-Atmos.*, 121, 6336–6355, 2016b.
- Heus, T. and Jonker, H. J.: Subsiding shells around shallow cumulus clouds, *J. Atmos. Sci.*, 65, 1003–1018, 2008.
- Holland, J. Z. and Rasmusson, E. M.: Measurements of the atmospheric mass, energy, and momentum budgets over a 500-kilometer square of tropical ocean, *Mon. Weather Rev.*, 101, 44–55, 1973.
- Holloway, C. E. and Neelin, J. D.: Moisture vertical structure, column water vapor, and tropical deep convection, *J. Atmos. Sci.*, 66, 1665–1683, 2009.
- Jaenicke, R.: Aerosol physics and chemistry, *Landolt-Börnstein Neue Serie*, 4b, 391–457, 1988.
- Jiang, H. L. and Feingold, G.: Effect of aerosol on warm convective clouds: Aerosol-cloud-surface flux feedbacks in a new coupled large eddy model, *J. Geophys. Res.-Atmos.*, 111, D01202, <https://doi.org/10.1029/2005jd006138>, 2006.
- Jiang, H., Xue, H., Teller, A., Feingold, G., and Levin, Z.: Aerosol effects on the lifetime of shallow cumulus, *Geophys. Res. Lett.*, 33, L14806, <https://doi.org/10.1029/2006gl026024>, 2006.
- Jiang, H., Feingold, G., and Sorooshian, A.: Effect of aerosol on the susceptibility and efficiency of precipitation in warm trade cumulus clouds, *J. Atmos. Sci.*, 67, 3525–3540, 2010.
- Johnson, R. H., Rickenbach, T. M., Rutledge, S. A., Ciesielski, P. E., and Schubert, W. H.: Trimodal characteristics of tropical convection, *J. Climate*, 12, 2397–2418, 1999.
- Kaufman, Y. J., Koren, I., Remer, L. A., Rosenfeld, D., and Rudich, Y.: The effect of smoke, dust, and pollution aerosol on shallow cloud development over the Atlantic Ocean, *P. Natl. Acad. Sci. USA*, 102, 11207–11212, <https://doi.org/10.1073/pnas.0505191102>, 2005.
- Khain, A. P.: Notes on state-of-the-art investigations of aerosol effects on precipitation: a critical review, *Environ. Res. Lett.*, 4, 015004, <https://doi.org/10.1088/1748-9326/4/1/015004>, 2009.
- Khain, A. P., Ovchinnikov, M., Pinsky, M., Pokrovsky, A., and Krugliak, H.: Notes on the state-of-the-art numerical modeling of cloud microphysics, *Atmos. Res.*, 55, 159–224, [https://doi.org/10.1016/S0169-8095\(00\)00064-8](https://doi.org/10.1016/S0169-8095(00)00064-8), 2000.
- Khain, A. and Pokrovsky, A.: Simulation of effects of atmospheric aerosols on deep turbulent convective clouds using a spectral microphysics mixed-phase cumulus cloud model. Part II: Sensitivity study, *J. Atmos. Sci.*, 61, 2983–3001, <https://doi.org/10.1175/jas-3281.1>, 2004.
- Khairoutdinov, M. F. and Randall, D. A.: Cloud resolving modeling of the ARM summer 1997 IOP: Model formulation, results, uncertainties, and sensitivities, *J. Atmos. Sci.*, 60, 607–625, 2003.
- Kogan, Y. L. and Martin, W. J.: Parameterization of bulk condensation in numerical cloud models, *J. Atmos. Sci.*, 51, 1728–1739, 1994.
- Koren, I., Kaufman, Y. J., Remer, L. A., and Martins, J. V.: Measurement of the effect of Amazon smoke on inhibition of cloud formation, *Science*, 303, 1342–1345, <https://doi.org/10.1126/science.1089424>, 2004.
- Koren, I., Kaufman, Y. J., Rosenfeld, D., Remer, L. A., and Rudich, Y.: Aerosol invigoration and restructuring of Atlantic convective clouds, *Geophys. Res. Lett.*, 32, L14828, <https://doi.org/10.1029/2005gl023187>, 2005.
- Koren, I., Martins, J. V., Remer, L. A., and Afargan, H.: Smoke invigoration versus inhibition of clouds over the Amazon, *Science*, 321, 946–949, <https://doi.org/10.1126/science.1159185>, 2008a.
- Koren, I., Oreopoulos, L., Feingold, G., Remer, L. A., and Altaratz, O.: How small is a small cloud?, *Atmos. Chem. Phys.*, 8, 3855–3864, <https://doi.org/10.5194/acp-8-3855-2008>, 2008b.
- Koren, I., Altaratz, O., Feingold, G., Levin, Z., and Reisin, T.: Cloud's Center of Gravity – a compact approach to analyze convective cloud development, *Atmos. Chem. Phys.*, 9, 155–161, <https://doi.org/10.5194/acp-9-155-2009>, 2009.
- Koren, I., Altaratz, O., Remer, L. A., Feingold, G., Martins, J. V., and Heiblum, R. H.: Aerosol-induced intensification of rain from the tropics to the mid-latitudes, *Nat. Geosci.*, 5, 118–122, 2012.
- Koren, I., Dagan, G., and Altaratz, O.: From aerosol-limited to invigoration of warm convective clouds, *Science*, 344, 1143–1146, 2014.
- Koren, I., Altaratz, O., and Dagan, G.: Aerosol effect on the mobility of cloud droplets, *Environ. Res. Lett.*, 10, 104011, <https://doi.org/10.1088/1748-9326/10/10/104011>, 2015.

- Kuang, Z. and Bretherton, C. S.: A mass-flux scheme view of a high-resolution simulation of a transition from shallow to deep cumulus convection, *J. Atmos. Sci.*, 63, 1895–1909, 2006.
- Lee, S.-S., Feingold, G., and Chuang, P. Y.: Effect of aerosol on cloud–environment interactions in trade cumulus, *J. Atmos. Sci.*, 69, 3607–3632, 2012.
- Lee, S. S., Kim, B.-G., Lee, C., Yum, S. S., and Posselt, D.: Effect of aerosol pollution on clouds and its dependence on precipitation intensity, *Clim. Dynam.*, 42, 557–577, 2014.
- Levin, Z. and Cotton, W. R.: *Aerosol pollution impact on precipitation: A scientific review*, Springer Science & Business Media, New York, 2009.
- Li, Z., Niu, F., Fan, J., Liu, Y., Rosenfeld, D., and Ding, Y.: Long-term impacts of aerosols on the vertical development of clouds and precipitation, *Nat. Geosci.*, 4, 888–894, <https://doi.org/10.1038/ngeo1313>, 2011.
- Malkus, S. J.: Some results of a trade-cumulus cloud investigation, *J. Meteorol.*, 11, 220–237, 1954.
- Nitta, T. and Esbensen, S.: Heat and moisture budget analyses using BOMEX data, *Mon. Weather Rev.*, 102, 17–28, 1974.
- Pinsky, M., Mazin, I., Korolev, A., and Khain, A.: Supersaturation and diffusional droplet growth in liquid clouds, *J. Atmos. Sci.*, 70, 2778–2793, 2013.
- Roesner, S., Flossmann, A., and Pruppacher, H.: The effect on the evolution of the drop spectrum in clouds of the preconditioning of air by successive convective elements, *Q. J. Roy. Meteor. Soc.*, 116, 1389–1403, 1990.
- Rosenfeld, D.: TRMM observed first direct evidence of smoke from forest fires inhibiting rainfall, *Geophys. Res. Lett.*, 26, 3105–3108, <https://doi.org/10.1029/1999gl100606>, 1999.
- Rosenfeld, D.: Suppression of rain and snow by urban and industrial air pollution, *Science*, 287, 1793–1796, <https://doi.org/10.1126/science.287.5459.1793>, 2000.
- Rosenfeld, D., Lohmann, U., Raga, G. B., O’Dowd, C. D., Kulmala, M., Fuzzi, S., Reissell, A., and Andreae, M. O.: Flood or drought: How do aerosols affect precipitation?, *Science*, 321, 1309–1313, <https://doi.org/10.1126/science.1160606>, 2008.
- Saleeby, S. M., Herbener, S. R., van den Heever, S. C., and L’Ecuyer, T.: Impacts of Cloud Droplet–Nucleating Aerosols on Shallow Tropical Convection, *J. Atmos. Sci.*, 72, 1369–1385, 2015.
- Savane, O. S., Vant-Hull, B., Mahani, S., and Khanbilvardi, R.: Effects of Aerosol on Cloud Liquid Water Path: Statistical Method a Potential Source for Divergence in Past Observation Based Correlative Studies, *Atmosphere*, 6, 273–298, 2015.
- Seifert, A. and Heus, T.: Large-eddy simulation of organized precipitating trade wind cumulus clouds, *Atmos. Chem. Phys.*, 13, 5631–5645, <https://doi.org/10.5194/acp-13-5631-2013>, 2013.
- Seifert, A., Heus, T., Pincus, R., and Stevens, B.: Large-eddy simulation of the transient and near-equilibrium behavior of precipitating shallow convection, *Journal of Advances in Modeling Earth Systems*, 7.4, 1918–1937, 2015.
- Seigel, R. B.: Shallow Cumulus Mixing and Subcloud Layer Responses to Variations in Aerosol Loading, *J. Atmos. Sci.*, 71, 2581–2603, 2014.
- Seiki, T. and Nakajima, T.: Aerosol effects of the condensation process on a convective cloud simulation, *J. Atmos. Sci.*, 71, 833–853, 2014.
- Siebesma, A. P., Bretherton, C. S., Brown, A., Chlond, A., Cuxart, J., Duynkerke, P. G., Jiang, H., Khairoutdinov, M., Lewellen, D., and Moeng, C. H.: A large eddy simulation intercomparison study of shallow cumulus convection, *J. Atmos. Sci.*, 60, 1201–1219, 2003.
- Small, J. D., Chuang, P. Y., Feingold, G., and Jiang, H.: Can aerosol decrease cloud lifetime?, *Geophys. Res. Lett.*, 36, L16806, <https://doi.org/10.1029/2009GL038888>, 2009.
- Squires, P.: The microstructure and colloidal stability of warm clouds, *Tellus*, 10, 262–271, 1958.
- Squires, P. and Twomey, S.: The relation between cloud droplet spectra and the spectrum of cloud nuclei, *Geoph. Monog. Series*, 5, 211–219, 1960.
- Stevens, B.: On the growth of layers of nonprecipitating cumulus convection, *J. Atmos. Sci.*, 64, 2916–2931, 2007.
- Stevens, B. and Seifert, R.: Understanding macrophysical outcomes of microphysical choices in simulations of shallow cumulus convection, *J. Meteorol. Soc. Jpn.*, 86, 143–162, 2008.
- Stevens, B. and Feingold, G.: Untangling aerosol effects on clouds and precipitation in a buffered system, *Nature*, 461, 607–613, <https://doi.org/10.1038/nature08281>, 2009.
- Takemi, T., Hirayama, O., and Liu, C.: Factors responsible for the vertical development of tropical oceanic cumulus convection, *Geophys. Res. Lett.*, 31, L11109, <https://doi.org/10.1029/2004GL020225>, 2004.
- Tao, W.-K., Chen, J.-P., Li, Z., Wang, C., and Zhang, C.: Impact of aerosols on convective clouds and precipitation, *Rev. Geophys.*, 50, RG2001, <https://doi.org/10.1029/2011RG000369>, 2012.
- Trenberth, K. E., Fasullo, J. T., and Kiehl, J.: Earth’s global energy budget, *B. Am. Meteorol. Soc.*, 90, 311–323, 2009.
- Waite, M. L. and Khouider, B.: The deepening of tropical convection by congestus preconditioning, *J. Atmos. Sci.*, 67, 2601–2615, 2010.
- Warner, J. and Twomey, S.: The production of cloud nuclei by cane fires and the effect on cloud droplet concentration, *J. Atmos. Sci.*, 24, 704–706, 1967.
- Xue, H. W. and Feingold, G.: Large-eddy simulations of trade wind cumuli: Investigation of aerosol indirect effects, *J. Atmos. Sci.*, 63, 1605–1622, <https://doi.org/10.1175/jas3706.1>, 2006.
- Xue, H. W., Feingold, G., and Stevens, B.: Aerosol effects on clouds, precipitation, and the organization of shallow cumulus convection, *J. Atmos. Sci.*, 65, 392–406, <https://doi.org/10.1175/2007jas2428.1>, 2008.
- Yin, Y., Carslaw, K. S., and Feingold, G.: Vertical transport and processing of aerosols in a mixed-phase convective cloud and the feedback on cloud development, *Q. J. Roy. Meteor. Soc.*, 131.605, 221–245, 2005.
- Yuan, T., Remer, L. A., and Yu, H.: Microphysical, macrophysical and radiative signatures of volcanic aerosols in trade wind cumulus observed by the A-Train, *Atmos. Chem. Phys.*, 11, 7119–7132, <https://doi.org/10.5194/acp-11-7119-2011>, 2011.
- Zhao, M. and Austin, P. H.: Life cycle of numerically simulated shallow cumulus clouds. Part I: Transport, *J. Atmos. Sci.*, 62, 1269–1290, <https://doi.org/10.1175/jas3414.1>, 2005.
- Zuidema, P., Li, Z., Hill, R. J., Bariteau, L., Rilling, B., Fairall, C., Brewer, W. A., Albrecht, B., and Hare, J.: On trade wind cumulus cold pools, *J. Atmos. Sci.*, 69, 258–280, 2012.